Letter

Structural criterion for the onset of rigidity in a colloidal gel

C. S. Dias,[1,2,*] J. C. Neves,[1,2,†] M. M. Telo da Gama,[1,2,‡] E. Del Gado,[3,§] and N. A. M. Araújo[1,2,‖]

[1]*Centro de Física Teórica e Computacional, Faculdade de Ciências, Universidade de Lisboa, 1749-016 Lisboa, Portugal*

[2]*Departamento de Física, Faculdade de Ciências, Universidade de Lisboa, 1749-016 Lisboa, Portugal*

[3]*Department of Physics, Institute for Soft Matter Synthesis and Metrology, Georgetown University, Washington, DC 20057, USA*

(Received 9 October 2024; revised 29 May 2025; accepted 5 June 2025; published 5 September 2025)

Identifying the conditions for rigidity onset in gels is challenging. We propose a model that distinguishes attractive bonds from repulsive steric constraints, allowing the systematic variation of the number of bonded and nonbonded neighbors. Using simulations, rheology, and percolation analysis, we find that rigidity coincides with the percolation of particles with three or more bonds, occurring after connectivity percolation. This interplay of bonding and steric interactions, which is not a local but a large-scale effect, provides the mechanism for the rigidity of low-valence colloidal gels.

DOI: 10.1103/gw42-dks6

Colloidal gels are nonequilibrium structures sustained by a percolating network of long-living bonds between the particles in solution [1–5]. They exhibit unique structural [6–9], dynamical [10–12], and mechanical [13–15] properties, which have motivated an intensive search for strategies to design them. This effort is relevant to food or cosmetics, and to energy materials or biotechnology and construction [16–20]. Recently, one focus has been on the design of low density gels and control of their local structures [21–33] using, e.g., vitrimetric materials or patchy particles, which limit the valence of the particles and the directionality of the bonds [34–37].

A key property of colloidal gels is their capacity to bear load without deforming permanently. However, the necessary condition for a gel to be rigid is still under debate [38]. This question is even more critical in the design of low-density gels, where the reduced number of bonds per particle may compromise the mechanical stability. During gelation, a percolating network of bonds emerges at a critical fraction of bonds per particle [1–5] but at this connectivity onset, the gels are floppy and fragile [39–41]. As more bonds are formed, a rigid elastic network emerges at a rigidity percolation transition [13,42]. It is difficult however to identify which subset of the visible structure is responsible for the stress transmission [13]. In 2D the onset of rigidity can be identified directly from the bond network with the pebble game algorithm [43–45], but in 3D the criteria remain elusive. Several local and global geometrical criteria have been proposed, such as a minimum average coordination number [40] or the existence of a directed percolating path [39], but a recently correlated rigidity percolation framework highlights the nonlocal nature of the emergence of rigidity, casting doubts on the previously proposed criteria [13].

Experiments combining confocal microscopy with microrheology in colloidal gels resulting from depletion forces suggest that the onset of rigidity coincides with the percolation of particles with at least six neighbors [46], in line with a local Maxwell rigidity criterion for isostaticity [47]. However recent experiments and simulations have clarified that this local criterion does not provide the necessary conditions for gel rigidity [38]. While attractive depletion forces are isotropic and pairs of bonded particles are free to rotate relative to each other [47], rotational degrees of freedom can be hindered by molecules grafted on the particle surfaces [48–50] and, quite generally, by more complex surface interactions [12,51,52].

Experimentally, the neighbor counting is based on the number of particles within a certain bonding distance. This definition is problematic for very short interaction ranges or when different types of interactions are present, as two neighboring particles are not necessarily bonded. We propose a different strategy, based on a patchy particle model where one can control attractive bonds from purely repulsive neighbors. Using this feature of the patchy particle model, and varying the number of attractive patches, we can proceed to analyze how the onset of rigidity depends on the number of neighbors, disentangling the contributions of bonded particles from those that only provide steric hindrance. We show that this difference is not a mere detail. For gels of limited valence, rigidity does emerge from the interplay of bonds and repulsive interactions (steric constraints). The onset of rigidity coincides with the emergence of a spanning aggregate of particles with at least three bonds for any value of the valence, including the isotropic continuum limit.

Colloidal particles with limited valence spontaneously form gels of very low density [53–57], with the focus of theoretical and numerical works being the connectivity percolation [21,58–61]. However, for most practical applications, the gel must be rigid. From the findings reported here, the relevant structural criterion is not the onset of connectivity percolation

*Contact author: csdias@fc.ul.pt
†Contact author: fc51402@alunos.fc.ul.pt
‡Contact author: mmgama@fc.ul.pt
§Contact author: emanuela.del.gado@georgetown.edu
‖Contact author: nmaraujo@fc.ul.pt

 ©2025 American Physical Society

but develops through the slow aging of the gel [13,38,62,63]. Specific local geometric motifs, which may depend on the particle interactions, contribute to attaining correlated rigidity percolation, however, it is their spatial organization and the way they are embedded in the structure that drives the onset of rigidity. Our results are consistent with recent findings for nanoparticle gels, providing further insight into the role of topological constraints [38,64]. The identification of the structural criterion for gel rigidity provides critical insight for designing gels tailored to specific applications.

Model. We consider a monodisperse suspension of spherical colloidal particles of radius R. The valence of each particle is limited by adding pointlike attractive sites equally spaced on the surface of the particles and consider that bonds are only established through the attractive sites. The number of attractive sites sets the valence. In most of this work the valence is set to three, however, we also study the effect of varying the valence. In all cases, the attractive sites are uniformly distributed on the surface of the colloid. The pairwise interaction is then a superposition of an isotropic repulsion and a site-site attraction (see the Supplemental Material [65]).

We first consider particles with three attractive sites on a cubic box of linear size $L = 32$ in units of the particle diameter and periodic boundary conditions in all directions. To form an elastic gel, number density is set to $\rho = 0.2$ and the thermostat temperature is such that $k_B T/\epsilon = 0.025$, where ϵ is the attractive interaction strength. The dynamics evolve over a total time of $10^3 \tau_B$, where $\tau_B = 4R^2/D_t$ is the Brownian time, and D_t is the diffusion coefficient. These parameters are chosen such that all particles are part of the gel. However, neither the values for the interaction parameters nor the softness of the potential affect the rheological measures in the regime of low frequency considered here (see the Supplemental Material [65]).

Rheological measurements. We minimize the energy by running zero-temperature overdamped simulations until the kinetic energy is, at least ten orders of magnitude lower than its initial value [63]. Then, we apply Lees-Edwards boundary conditions and an oscillatory affine shear deformation, parametrized by $\gamma(t) = \gamma_0 \sin(\omega t)$, with frequency ω and amplitude γ_0 (see the Supplemental Material [65]), and identify the linear regime from the load curve. To focus on that regime, we set $\gamma_0 = 0.07$. The first-order storage G_1' and loss G_1'' moduli are obtained from the time evolution of the shear stress $\sigma_{xy}(t)$ as in Ref. [63].

Figures 1(a)–1(c) are snapshots at different times, where the color of a particle corresponds to the number of bonded neighbors. Figures 1(d)–1(f) show the dependence of G_1' and G_1'' on ω, for the three different regimes of gelation, where each structure is relaxed at zero temperature and then subject to the oscillatory measurements. Initially, in (a) and (d), most particles have established either one or no bonds. G_1' is lower than G_1'' and it scales linearly with ω, as in a Maxwell-like fluid [66]. As time evolves, more bonds are established and aggregates are formed with a characteristic size of several particles, affecting the mechanical response. For (b) and (e), G_1' is still lower than G_1'' but both scale as ω^α, with $\alpha < 1$; We estimate $\alpha = 0.60 \pm 0.05$ [64]. Finally, in (c) and (f), a percolating network of particles with three bonds is already formed. Operationally, the gel is rigid when the storage

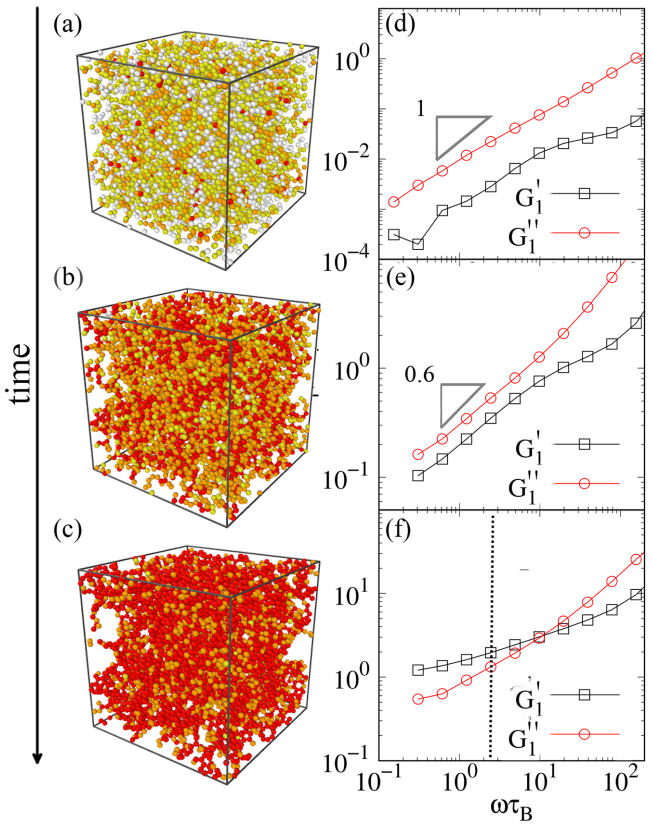

FIG. 1. Time dependence of the mechanical properties of a gel of spherical particles with valence three. (a)–(c) Three snapshots at different times. The color of each particle indicates its number of bonds: white (0), yellow (1), orange (2), and red (3). (d)–(f) The storage (G_1') and loss (G_1'') moduli at the same times. (a) and (d) correspond to a viscoelastic fluid, (b) and (e) to a soft glassy material, and (c) and (f) to an elastic gel. Mechanical properties were measured in one sample of a cubic box of linear size $L = 32$, in units of the particle diameter, and number density $\rho = 0.2$.

(elastic) modulus dominates over the loss (viscous) modulus at low enough frequencies [67].

The time dependence of G_1' and G_1'' for a frequency $\approx 2.5\ \tau_B^{-1}$ is shown in Fig. 2(a) [vertical line in Fig. 1(f)]. Both moduli increase with time, and the transition to an elastic gel ($G_1' \geqslant G_1''$) occurs around $10\tau_B$ (vertical red dashed line). The fraction of particles in the largest connected component is plotted in Fig. 2(b) (black curve). The onset of rigidity occurs much later than that for the onset of connectivity percolation (vertical black dashed line, from Ref. [68]). However, if we compute the size of the largest cluster of fully bonded particles (red circles curve), the data indicate that the onset of percolation of this subset coincides with the onset of rigidity.

To further test if the onset of rigidity coincides with the percolation threshold of particles with three bonds, we performed the following percolation analysis. We started from gel configurations at the final time of the simulations, when the gel is predominantly elastic and the particles with three bonds percolate. The kinetic energy is minimized as described in the protocol above. Then, at each iteration, one particle is selected and one of its attractive sites is removed. Both the particle and the attractive site are selected at random.

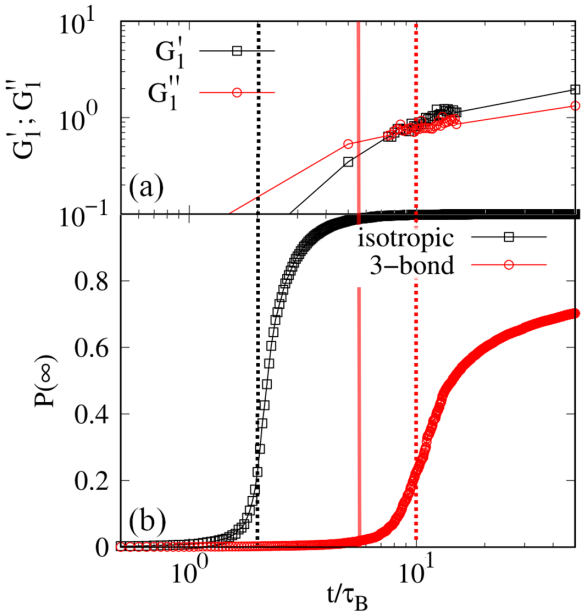

FIG. 2. Mechanical and percolation properties of a gel of spherical particles with valence three. (a) Storage G_1' and loss G_1'' moduli as a function of time, measured at a frequency corresponding to the vertical line in Fig. 1(f). (b) Fraction of particles, $P(\infty)$, in the largest connected component (black) and largest cluster of particles with three bonds (red) as a function of time. In (a) and (b), the vertical black (left) and red (right) dashed lines indicate the thresholds for the connectivity percolation considering all particles (left) and the percolation of particles with three bonds (right). The vertical solid line indicates the time at which $G' = G''$ for zero frequency. All simulations were performed on a cubic box of linear size $L = 32$, in units of the particle diameter, number density $\rho = 0.2$, and the results are averaged over ten samples for the percolation analysis and correspond to only one sample for the mechanical properties.

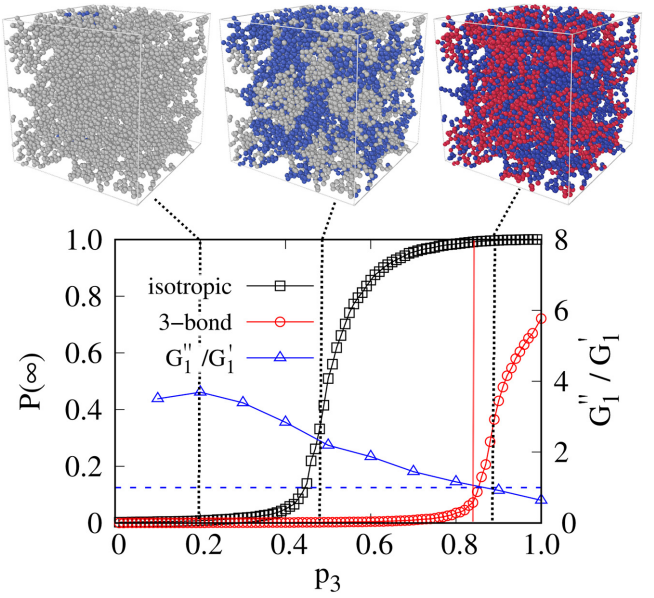

FIG. 3. Percolation analysis of the mechanical properties of a gel of spherical particles with initial valence three (maximum three bonds per particle), where sites are removed at random. Fraction of particles, $P(\infty)$, in the largest connected component (black squares) and largest cluster of particles with three bonds (red squares) as a function of the fraction of the remaining particles with three attractive sites p_3. Loss factor (blue triangles) $\tan(\delta) = G_1''/G_1'$ as a function of p_3. Top panel: Snapshots at three different stages (vertical dashed lines in the plot). Red particles are in the largest cluster of particles with three bonds (fully bonded), blue particles are in the largest connected component, and all the other particles are gray. The vertical solid line indicates the time at which $G' = G''$ for zero frequency. All simulations were performed on a cubic box of linear size $L = 32$, in units of the particle diameter, for a number density $\rho = 0.2$. The results are averaged over ten samples for the percolation analysis and correspond to only one sample for the mechanical properties.

The gel is not allowed to age, to keep the same structure. We evaluate the mechanical and percolation properties as a function of p_3, defined as the fraction of particles that still have three attractive sites. Figure 3 depicts the dependence on p_3 of the size of the largest connected component, the largest cluster of particles with three bonds and the ratio G_1'/G_1''. The data reveals that the onset of rigidity and the percolation of particles with three bonds coincide. Note that particles and attractive sites are selected uniformly at random, discarding possible effects from spatial correlations developed during the dynamics.

Effect of the valence. To evaluate the robustness of the three-bonded particle percolation criterium, we performed the same percolation analysis for gels of particles with number of bonds per particle (valence) *ns* from three to twelve, which is the number of neighbors in compact 3D packings (see Fig. S8 in the Supplemental Material [65]). We select particles at random and remove all of their attractive sites but two. Thus, at each iteration, the particles have either *ns* or two attractive sites. The onsets of connectivity and three-bonded particle percolation transitions depend strongly on the valence *ns*. While that for connectivity increases with *ns*, that for three-bonded particles shifts to lower values of p_{ns}. Thus, for particles with higher valence, the two transitions would be very difficult to distinguish experimentally. As in the system with $ns = 3$ (Fig. 3), the G_1' is only larger than G_1'' above the percolation transition for particles with at least three bonds. Below this transition, G_1'' is the largest, over the entire range of frequencies, and thus the gel is rather a viscous fluid. Even at high valence, the percolation of three-bonded particles is still a valid criterion. One may therefore expect it to remain valid in the continuum limit for unconstrained valence.

Bonds versus steric constraints. A snapshot of the largest connected component at the onset of rigidity is shown in Fig. 4(a), where the set of fully bonded (three bonds) particles is represented by the network of bonds (red). The cluster of three-bonded particles forms a spanning network with very low average connectivity and cycles of at least five particles. We study the effect of the two types of interactions: steric constraints (repulsive contacts) and bonds. In Fig. 4(b), we plot G_1' and G_1'' for the cluster of three-bonded particles, neglecting the interaction with particles outside that cluster during the rheological measurements. We observe that this structure is not rigid. Even considering all particles, switching off the repulsive steric constraints while keeping the attractive bonds, results in a nonrigid structure [see Fig. 4(c)]. Only when

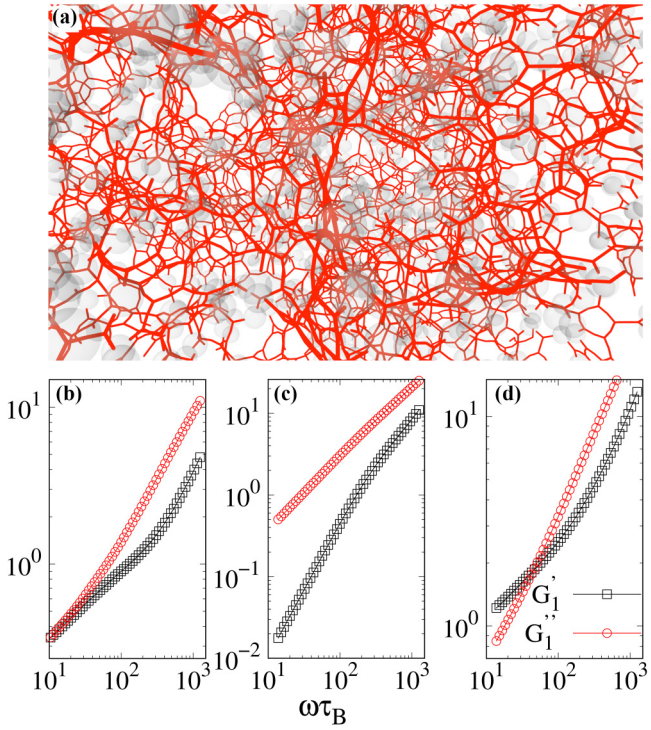

FIG. 4. Structure and mechanical properties of the cluster of three-bonded particles. (a) Snapshot of the largest connected component at the onset of rigidity, where the cluster of particles with three bonds is represented by the network of bonds (red) and all the other particles are in gray. (b), (c), and (d) are the storage G_1' and loss G_1'' moduli as a function of the frequency ω. (b) depicts the cluster of particles with three bonds (red network), (c) the largest connected component when we switch off the repulsive interactions, between all particles, during the rheological measurements, and (d) the largest connected component when we switch off the repulsive interaction only between the particles with less than three bonds during the rheological measurements. All simulations were performed on a cubic box of linear size $L = 32$, in units of particle diameter, and number density $\rho = 0.2$, for one sample.

including the repulsive steric constraints of particles with three bonds the structure becomes rigid [see Fig. 4(d)]. Thus, although the onset of rigidity coincides with the percolation of particles with three bonds, rigidity requires a combination of bonds and repulsive (steric) interactions. This combination does not depend on local interactions (see Figs. S2 and S3 in the Supplemental Material [65]), but rather on a large-scale steric effect that stabilizes the gel.

Effect of bond sliding. We now consider the effect of bond sliding, assuming a bending energy described by a quadratic potential $V_\theta = k_A(\theta - \theta_0)^2$, where θ is the angle between the bonds at the center of the particle. The equilibrium angle θ_0 is $2\pi/3$, and k_A is the strength of the bending energy (results in Figs. S9 and S10 in the Supplemental Material [65]). In the absence of bending energy ($k_A = 0$), the bonds are free to move around the particle, and the gel is never rigid. Otherwise, the gel is rigid for all $k_A \neq 0$ and the transition frequency vanishes for $k_A = 0$, that is, in the absence of bending energy. This is consistent with what was found for fiber networks [69]. A nonmonotonic dependence of the frequency transition as a function of k_A was found, indicating a competition between the rigidity promoted by the bond resistance to sliding and the local rearrangement to more stable (rigid) positions when sliding is allowed.

Conclusion. It is the combination of network bonds and steric constraints that leads to the rigidity of the gel. The development of rigid structures depends strongly on the gelation dynamics, not just on the number of bonds of a particle, as proposed by correlated rigidity percolation [13]. For all the gels considered here, where the particle valence ranged from three to twelve, we found that the onset of gel rigidity corresponds to the percolation of particles with at least three bonds, suggesting that for the type of interactions considered, this identifies the necessary condition for rigidity percolation. For nanoparticles with ad hoc limited valence, our results show that a sufficient fraction of particles with valence three is required to design rigid structures. More generally, when the valence cannot be controlled precisely, our findings shed light on how the mechanics of colloidal gels result from the interplay of different substructures intertwined with each other, not easily recognizable from local geometrical motifs [70]. The implications of our discoveries extend far beyond the study of colloidal gels. From biomaterials to advanced manufacturing and beyond, the ability to predict and control gel rigidity opens avenues for the design of customizable materials with targeted mechanical properties. Consider biomedical applications where gels must provide structural support within the body [20,71] or act as drug delivery systems [72], which, by using low-density gels of limited-valence particles, one could understand and manipulate rigidity to revolutionize treatment strategies.

Acknowledgments. We acknowledge financial support from the Portuguese Foundation for Science and Technology (FCT) under Contracts No. PTDC/FIS-MAC/28146/2017 (LISBOA-01-0145-FEDER-028146), No. PTDC/FIS-MAC/5689/2020, No. EXPL/FIS-MAC/0406/2021 [73], No. CEECIND/00586/2017, No. UIDB/00618/2020, and No. UIDP/00618/2020. E.D.G. acknowledges financial support from National Science Foundation (NSF) DMR-2026842. The authors also thank Minaspi Bantawa for support with the rheological tests.

[1] P. J. Lu, E. Zaccarelli, F. Ciulla, A. B. Schofield, F. Sciortino, and D. A. Weitz, Nature (London) **453**, 499 (2008).

[2] P. N. Pusey and W. van Megen, Nature (London) **320**, 340 (1986).

[3] D. Bonn, H. Tanaka, G. Wegdam, H. Kellay, and J. Meunier, Europhys. Lett. **45**, 52 (1999).

[4] C. L. Klix, C. P. Royall, and H. Tanaka, Phys. Rev. Lett. **104**, 165702 (2010).

[5] A. M. Puertas, M. Fuchs, and M. E. Cates, Phys. Rev. Lett. **88**, 098301 (2002).
[6] C. Ferreiro-Córdova, E. Del Gado, G. Foffi, and M. Bouzid, Soft Matter **16**, 4414 (2020).
[7] S. Griffiths, F. Turci, and C. P. Royall, J. Chem. Phys. **146**, 014905 (2017).
[8] J. Colombo, A. Widmer-Cooper, and E. Del Gado, Phys. Rev. Lett. **110**, 198301 (2013).
[9] S. Machlus, S. Zhang, and X. Mao, Phys. Rev. E **103**, 012104 (2021).
[10] J. H. Cho, R. Cerbino, and I. Bischofberger, Phys. Rev. Lett. **124**, 088005 (2020).
[11] J. M. Tavares, C. S. Dias, N. A. M. Araújo, and M. M. Telo da Gama, J. Phys. Chem. B **122**, 3514 (2018).
[12] F. Bonacci, X. Chateau, E. M. Furst, J. Fusier, J. Goyon, and A. Lemaître, Nat. Mater. **19**, 775 (2020).
[13] S. Zhang, L. Zhang, M. Bouzid, D. Z. Rocklin, E. Del Gado, and X. Mao, Phys. Rev. Lett. **123**, 058001 (2019).
[14] J. Colombo and E. Del Gado, Soft Matter **10**, 4003 (2014).
[15] H. Tsurusawa, S. Arai, and H. Tanaka, Sci. Adv. **6**, eabb8107 (2020).
[16] S. Mitura, A. Sionkowska, and A. Jaiswal, J. Mater. Sci.: Mater. Med. **31**, 50 (2020).
[17] K. Ioannidou, M. Kanduč, L. Li, D. Frenkel, J. Dobnikar, and E. Del Gado, Nat. Commun. **7**, 12106 (2016).
[18] S. Banerjee and S. Bhattacharya, Crit. Rev. Food Sci. Nutr. **52**, 334 (2012).
[19] I. Coropceanu, E. M. Janke, J. Portner, D. Haubold, T. D. Nguyen, A. Das, C. P. N. Tanner, J. K. Utterback, S. W. Teitelbaum, M. H. Hudson, N. A. Sarma, A. M. Hinkle, C. J. Tassone, A. Eychmüller, D. T. Limmer, M. Olvera de la Cruz, N. S. Ginsberg, and D. V. Talapin, Science **375**, 1422 (2022).
[20] C. S. Dias, C. A. Custodio, G. C. Antunes, M. M. Telo da Gama, J. F. Mano, and N. A. Araujo, ACS Appl. Mater. Interfaces **12**, 48321 (2020).
[21] B. Ruzicka, E. Zaccarelli, L. Zulian, R. Angelini, M. Sztucki, A. Moussaïd, T. Narayanan, and F. Sciortino, Nat. Mater. **10**, 56 (2011).
[22] E. Bianchi, J. Largo, P. Tartaglia, E. Zaccarelli, and F. Sciortino, Phys. Rev. Lett. **97**, 168301 (2006).
[23] F. Smallenburg and F. Sciortino, Nat. Phys. **9**, 554 (2013).
[24] A. B. Pawar and I. Kretzschmar, Macromol. Rapid Commun. **31**, 150 (2010).
[25] K. J. Lee, J. Yoon, and J. Lahann, Curr. Opin. Colloid Interface Sci. **16**, 195 (2011).
[26] Z. He and I. Kretzschmar, Langmuir **28**, 9915 (2012).
[27] Y. Wang, Y. Wang, X. Zheng, É. Ducrot, J. S. Yodh, M. Weck, and D. J. Pine, Nat. Commun. **6**, 7253 (2015).
[28] A. A. Shah, B. Schultz, K. L. Kohlstedt, S. C. Glotzer, and M. J. Solomon, Langmuir **29**, 4688 (2013).
[29] E. Bianchi, B. Capone, G. Kahl, and C. N. Likos, Faraday Discuss. **181**, 123 (2015).
[30] F. Romano, E. Sanz, and F. Sciortino, J. Chem. Phys. **134**, 174502 (2011).
[31] O. Markova, J. Alberts, E. Munro, and P.-F. Lenne, Phys. Rev. E **90**, 022301 (2014).
[32] D. Ortiz, K. L. Kohlstedt, T. D. Nguyen, and S. C. Glotzer, Soft Matter **10**, 3541 (2014).
[33] J. R. Wolters, G. Avvisati, F. Hagemans, T. Vissers, D. J. Kraft, M. Dijkstra, and W. K. Kegel, Soft Matter **11**, 1067 (2015).
[34] F. Smallenburg, L. Leibler, and F. Sciortino, Phys. Rev. Lett. **111**, 188002 (2013).
[35] Q. L. Lei, X. Xia, J. Yang, M. P. Ciamarra, and R. Ni, Proc. Natl. Acad. Sci. USA **117**, 27111 (2020).
[36] M. Capelot, M. M. Unterlass, F. Tournilhac, and L. Leibler, ACS Macro Lett. **1**, 789 (2012).
[37] M. Liu, X. Zheng, V. Grebe, D. J. Pine, and M. Weck, Nat. Mater. **19**, 1354 (2020).
[38] S. M. Fenton, P. Padmanabhan, B. K. Ryu, T. T. D. Nguyen, R. N. Zia, and M. E. Helgeson, Proc. Natl. Acad. Sci. USA **120**, e2215922120 (2023).
[39] M. Kohl, R. F. Capellmann, M. Laurati, S. U. Egelhaaf, and M. Schmiedeberg, Nat. Commun. **7**, 11817 (2016).
[40] N. E. Valadez-Pérez, Y. Liu, A. P. R. Eberle, N. J. Wagner, and R. Castañeda-Priego, Phys. Rev. E **88**, 060302(R) (2013).
[41] J. J. Richards, J. B. Hipp, J. K. Riley, N. J. Wagner, and P. D. Butler, Langmuir **33**, 12260 (2017).
[42] C. I. N. S. Filho, J. S. Andrade, Jr., H. J. Herrmann, and A. A. Moreira, Phys. Rev. Lett. **120**, 175701 (2018).
[43] D. J. Jacobs and M. F. Thorpe, Phys. Rev. Lett. **75**, 4051 (1995).
[44] W. G. Ellenbroek, V. F. Hagh, A. Kumar, M. F. Thorpe, and M. van Hecke, Phys. Rev. Lett. **114**, 135501 (2015).
[45] E. Berthier, J. E. Kollmer, S. E. Henkes, K. Liu, J. M. Schwarz, and K. E. Daniels, Phys. Rev. Mater. **3**, 075602 (2019).
[46] H. Tsurusawa, M. Leocmach, J. Russo, and H. Tanaka, Sci. Adv. **5**, eaav6090 (2019).
[47] R. Blumenfeld, S. F. Edwards, and R. C. Ball, J. Phys.: Condens. Matter **17**, S2481 (2005).
[48] L. Feng, R. Dreyfus, R. Sha, N. C. Seeman, and P. M. Chaikin, Adv. Mater. **25**, 2779 (2013).
[49] S. Sacanna, M. Korpics, K. Rodriguez, L. Colón-Meléndez, S.-H. Kim, D. J. Pine, and G.-R. Yi, Nat. Commun. **4**, 1688 (2013).
[50] Y. Wang, D. R. Breed, V. N. Manoharan, L. Feng, A. D. Hollingsworth, M. Weck, and D. J. Pine, Nature (London) **491**, 51 (2012).
[51] M. Bantawa, W. A. Fontaine-Seiler, P. D. Olmsted, and E. Del Gado, J. Phys.: Condens. Matter **33**, 414001 (2021).
[52] B. van der Meer, T. Yanagishima, and R. P. A. Dullens, Phys. Rev. Lett. **134**, 078202 (2025).
[53] J. Russo, P. Tartaglia, and F. Sciortino, J. Chem. Phys. **131**, 014504 (2009).
[54] N. A. M. Araújo, C. S. Dias, and M. M. Telo da Gama, J. Phys.: Condens. Matter **29**, 014001 (2017).
[55] D. de las Heras, J. M. Tavares, and M. M. Telo da Gama, Soft Matter **8**, 1785 (2012).
[56] J. Russo, J. M. Tavares, P. I. C. Teixeira, M. M. Telo da Gama, and F. Sciortino, Phys. Rev. Lett. **106**, 085703 (2011).
[57] J. Russo, F. Leoni, F. Martelli, and F. Sciortino, Rep. Prog. Phys. **85**, 016601 (2022).
[58] M. P. Howard, R. B. Jadrich, B. A. Lindquist, F. Khabaz, R. T. Bonnecaze, D. J. Milliron, and T. M. Truskett, J. Chem. Phys. **151**, 124901 (2019).
[59] E. Zaccarelli, S. V. Buldyrev, E. La Nave, A. J. Moreno, I. Saika-Voivod, F. Sciortino, and P. Tartaglia, Phys. Rev. Lett. **94**, 218301 (2005).
[60] E. Zaccarelli, I. Saika-Voivod, S. V. Buldyrev, A. J. Moreno, P. Tartaglia, and F. Sciortino, J. Chem. Phys. **124**, 124908 (2006).

[61] E. Bianchi, R. Blaak, and C. N. Likos, Phys. Chem. Chem. Phys. **13**, 6397 (2011).
[62] C. S. Dias, J. M. Tavares, N. A. M. Araújo, and M. M. Telo da Gama, Soft Matter **14**, 2744 (2018).
[63] J. Colombo and E. Del Gado, J. Rheol. **58**, 1089 (2014).
[64] M. Bantawa, B. Keshavarz, M. Geri, M. Bouzid, T. Divoux, G. H. McKinley, and E. Del Gado, Nat. Phys. **19**, 1178 (2023).
[65] See Supplemental Material at http://link.aps.org/supplemental/10.1103/gw42-dks6 for additional information about the model and results.
[66] T. G. Mason and D. A. Weitz, Phys. Rev. Lett. **74**, 1250 (1995).
[67] R. G. Larson, *The Structure and Rheology of Complex Fluids* (Oxford University Press, New York, 1991).
[68] C. S. Dias, N. A. M. Araújo, and M. M. Telo da Gama, J. Phys.: Condens. Matter **30**, 014001 (2018).
[69] C. P. Broedersz, X. Mao, T. C. Lubensky, and F. C. Mackintosh, Nat. Phys. **7**, 983 (2011).
[70] J. C. Neves, J. M. Tavares, N. A. M. Araújo, and C. S. Dias, companion paper, Phys. Rev. E **112**, 035406 (2025).
[71] C. A. Custódio, M. T. Cerqueira, A. P. Marques, R. L. Reis, and J. F. Mano, Biomaterials **43**, 23 (2015).
[72] L. Lei, Y. Bai, X. Qin, J. Liu, W. Huang, and Q. Lv, Gels **8**, 301 (2022).
[73] https://doi.org/10.54499/PTDC/FIS-MAC/5689/2020.